Analysis of ^{27}Al- and ^{93}Nb-NMR spectra of $PrNb_2Al_{20}$ single crystal

Tetsuro Kubo[1,*], Hisashi Kotegawa[1], Hideki Tou[1,†]
Ryuji Higashinaka[2], Akihiro Nakama[2], Yuji Aoki[2], and Hideyuki Sato[2]

[1]Department of Physics, Graduate School of Science, Kobe University, 1-1 Rokkodai, Kobe, Hyogo 657-8501, Japan
[2]Department of Physics, Graduate School of Science and Engineering, Tokyo Metropolitan University, 1-1 Minamiohsawa, Hachioji, Tokyo 192-0397, Japan

E-mail: *tkubo@stu.kobe-u.ac.jp †tou@crystal.kobe-u.ac.jp

Abstract. We report the results of ^{27}Al- and ^{93}Nb- nuclear magnetic resonance (NMR) and nuclear quadrupole resonance (NQR) measurements in $PrNb_2Al_{20}$ single crystals. The field angle dependence of the observed ^{93}Nb-NMR lines for the single crystal at around 5 T and at 50 K is reproduced by a simulation using previously reported NQR parameters $\nu_{Q,Nb} \approx 1.82$ MHz and $\eta_{Nb} \approx 0$, while ^{27}Al-NMR lines were not reproduce by the previously reported NQR parameters $\nu_{Q,Al(3)} \approx 1.53$ MHz and $\eta_{Al(3)} \approx 0.17$. By reexamining and reconsidering the NMR and NQR lines for powder samples, we obtained a correct NQR parameters for Al(3) site to be $\nu_{Q,Al(3),new} \approx 1$ MHz and $\eta_{Al(3),new} \approx 0.4$.

1. Introduction

Pr-based cubic intermetallic compound PrT_2X_{20} (T = Ir, Rh, Ti, V, Nb, X = Zn, Al) shows various interesting behaviors such as quadrupole order, unconventional superconductivity and non-Fermi liquid (NFL) behavior [1, 2, 3, 4, 5, 6]. In this system, $4f$ electrons can have a nonmagnetic but multipole active crystalline electric field (CEF) ground state because of the cubic CEF effect with T_d point symmetry. Such a CEF ground state is characterized by Γ_3 doublet that has no magnetic dipole moment but has two electric quadrupole moment O_{20} and O_{22} and one magnetic octupole moment T_{xyz}. These multipole degrees of freedom are considered to be a key to understanding the intriguing phenomena at low temperatures in the PrT_2X_{20}.

In the PrT_2X_{20} series, it is shown that $PrNb_2Al_{20}$ does not show any phase transition down to 75 mK by bulk and nuclear quadrupole resonance (NQR) measurements [7, 8]. In addition, this compound shows NFL behaviors such as T-linear resistivity and logarithmic divergent specific heat divided by temperature at low temperatures below 2 K [3]. The relationship between these anomalous behaviors and the multipole degrees of freedom has been discussed in this compound [7, 8].

In order to investigate the low-energy excitation of the multipoles in $PrNb_2Al_{20}$, nuclear magnetic resonance (NMR) and NQR are desirable because these methods can obtain the information of the local electronic state from static and dynamic viewpoints. We have already reported possible NQR parameters at Al site from the ^{27}Al-NMR results measured at 30 K and around 2.8 T for a powder sample [9]. In the previous study, we assumed that the contributions of the hyperfine and classical dipolar interactions are negligible compared to the electric quadrupole interactions.

$PrNb_2Al_{20}$ has the cubic $CeCr_2Al_{20}$-type structure with the space group $Fd\bar{3}m$: Pr atoms at 8a site are encapsulated in highly symmetric Al_{16} cages, so called the Frank-Kasper cage formed by four Al(1) atoms and twelve Al(3) atoms. Note that Al atoms in 1-2-20 system have three crystallographically inequivalent Al sites; Al(1) is in the position of trigonal 16c site; Al(2) is in the orthorombic 48f site; Al(3) is in the monoclinic 96g site. Another structural aspect to be noted is that the Nb atoms at the trigonal 16d site form a pyrochlore lattice. Therefore, it is difficult to determine the electric field gradient (EFG) tensors at NMR active Al and Nb sites only by the powder NMR spectrum. Before discussing NMR results in detail, we need to gain a detailed EFG parameters. In this paper, we report the results of ^{93}Nb-NMR measurements using a single crystal and reanalysis of ^{27}Al-NMR results for the powder sample. In the present study, we have found that contributions from dipolar and hyperfine interactions are important to discuss the NMR line profile as well as field and temperature dependences of the NMR spectrum. Thus we have reexamined and reanalyzed the ^{27}Al-NMR powder spectrum together with ^{93}Nb-NMR measurements using a single crystal sample.

2. Experimental procedure

Single crystal samples of $PrNb_2Al_{20}$were prepared by Al-flux method. Details of sample preparation method are reported in the previous paper [3]. Field angle dependence of NMR lines are measured by using a single crystal sample that has the dimension of $\sim 2 \times 2 \times 2\,\mathrm{mm}^3$. To estimate NQR parameters, measurements were performed using powder samples, in which single crystal samples were crushed into powder form in order to gain signal intensity. NMR measurements were performed using 12 T and 17 T superconducting magnets and a phase-coherent pulsed spectrometer at magnetic fields around $\mu_0 H = 2.8$ and 5 T. ^{93}Nb- (nuclear spin $I = 9/2$, nuclear gyromagnetic ratio $^{93}\gamma_n/2\pi = 10.452\,\mathrm{MHz/T}$, and nuclear quadrupole moment $Q = -0.320\times10^{-28}\,\mathrm{m}^{-2}$) and ^{27}Al- ($I = 5/2$, $^{27}\gamma_n/2\pi = 11.103\,\mathrm{MHz/T}$, and $Q = -0.1466\times10^{-28}\,\mathrm{m}^{-2}$) NMR spectra were obtained by tracing spin-echo intensity as a function of the resonance field.

3. Results and discussion

First, we discuss the ^{93}Nb-NMR spectrum for a single crystal. Figure 1 shows a field swept NMR spectrum measured at a fixed frequency of $f = 48.751$ MHz and 50 K for the applied field nearly parallel to $\langle 110\rangle$. The linewidth of the obtained NMR lines is narrow about 30 G at around 5 T, and the each line splits well.

To reproduce the observed ^{93}Nb-NMR spectrum, the resonance fields were calculated by an exact diagonalization of the $(2I+1)\times(2I+1)$ nuclear spin hamiltonian [10],

$$\mathcal{H} = -\gamma_n\hbar\boldsymbol{I}\cdot\boldsymbol{H}_0 - \gamma_n\hbar\boldsymbol{I}\cdot\tilde{K}\cdot\boldsymbol{H}_0 - \gamma_n\hbar\boldsymbol{I}\cdot\boldsymbol{H}_d + \frac{1}{6}h\nu_Q\left\{3I_Z^2 - I(I+1) + \frac{\eta}{2}(I_+^2 + I_-^2)\right\} \tag{1}$$

where h is Planck constant and $\hbar \equiv h/2\pi$. The first term is the Zeeman term between the nuclear spin $\boldsymbol{I}$ and the applied field $\boldsymbol{H}_0$. The second term shows a hyperfine interaction between the nuclear spin and electrons. $\tilde{K}$ is a second rank Knight shift tensor, which includes an isotropic part K_{iso} and an anisotropic part K_i ($i = 1, 2, 3$). The anisotropic part is defined so as to fulfill the relations $\sum_i K_i = 0$ and $|K_3| \geq |K_2| \geq |K_1|$. The third term represents a classical dipole field contribution between the nuclear spin and the localized Pr-$4f$ moment $\boldsymbol{\mu}_i = -g_J\mu_B\boldsymbol{J}_i$ at the ith Pr site, where g_J, μ_B, and $\boldsymbol{J}_i$ are Landé g-factor, Bohr magneton, and the $4f$ electron spin matrix, respectively. The dipole field at Nb, Al(1), Al(2), and Al(3) site is calculated by summing up the contributions of $11\times11\times11$ neighboring Pr atoms in the lattice as

$$\boldsymbol{H}_d = \sum_i\left[-\frac{\boldsymbol{\mu}_i}{r_i} + \frac{3(\boldsymbol{\mu}\cdot\boldsymbol{r}_i)\,\boldsymbol{r}_i}{r_i^5}\right], \tag{2}$$

where r_i is the distance between the site concerned and the ith Pr $4f$ moment. For instance, when we applied the magnetic field parallel to $\langle 001\rangle$ direction, $|\boldsymbol{H}_d|$ for each site is obtained to be $|\boldsymbol{H}_{d,Nb}| \approx 8$ Oe, $|\boldsymbol{H}_{d,Al(2)}| \approx 10$ Oe, and $|\boldsymbol{H}_{d,Al(3)}| \approx 40$ Oe.

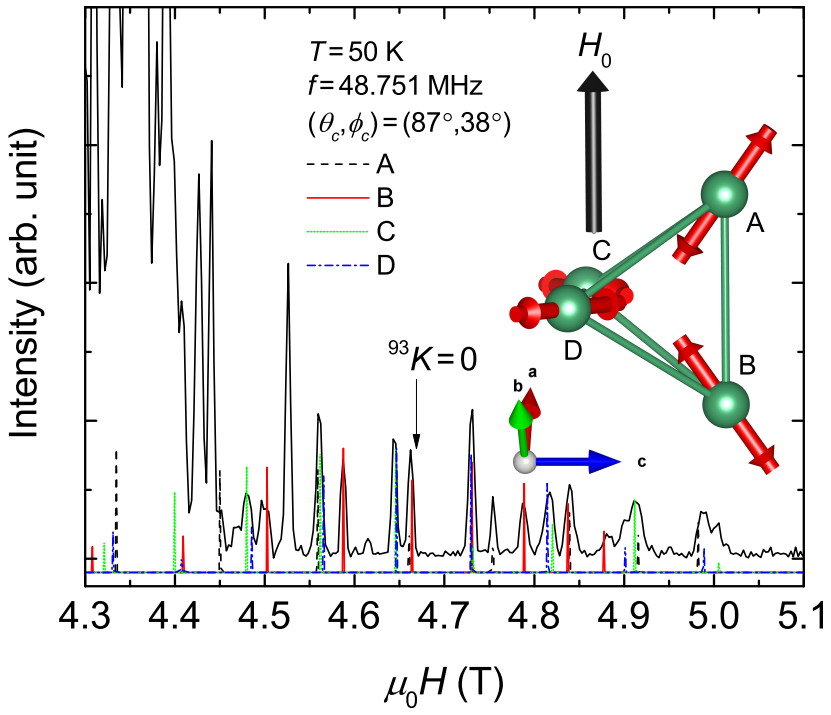

Figure 1. ^{93}Nb- and ^{27}Al-NMR lines obtained for a fixed frequency of 48.751 MHz and 50 K for a field nearly parallel to ⟨110⟩ direction of the crystal axes. The black dashed, red solid, green dotted, and blue dashed-dotted lines are the result of the simulation assuming that the magnetic field is applied for $(\theta_C, \phi_C) = (87°, 38°)$ direction. (θ_C, ϕ_C) are the polar angles between ⟨100⟩ direction and the applied field direction. The black arrow indicates the origin of the ^{93}Nb Knight shift. The inset shows four neighboring Nb sites. When the magnetic field is applied along ⟨110⟩ direction indicated by a black arrow, two inequivalent Nb sites (A, B) and (C, D) appear. Red arrows denotes V_{ZZ} directions that are parallel to one of ⟨111⟩ directions. Unassigned lines come from ^{27}Al nuclei.

The fourth term is the electric quadrupole interaction. Here $\nu_Q \equiv 3eQV_{ZZ}/2hI(2I-1)$ is a nuclear quadrupole frequency, where e is unit charge, $\eta \equiv (V_{XX} - V_{YY})/V_{ZZ}$ is an asymmetry parameter, and $V_{\alpha\alpha}$ $(\alpha = X, Y, Z)$ are principal values of the electric field gradient (EFG) tensor defined to be $|V_{ZZ}| \geq |V_{YY}| \geq |V_{XX}|$, so as $0 \leq \eta \leq 1$. Note that the quantization axis is taken as the principal axes of the nuclear quadrupole interaction.

As mentioned above, the Nb site has axial symmetry and the maximum principal axes of the the Knight shift (K), classical dipole (D), and nuclear quadrupole interaction (Q) direct one of the ⟨111⟩ directions of the crystal coordinate (C) as shown in the inset of Fig. 1. In this case, we can take K, D, and Q coordinates to coincide.

In order to calculate NMR lines for an arbitrary field angle with respect to the crystal axis, we should perform a frame transformation from C, K, D, and Q coordinates to the Zeeman (Z) coordinates. We define the field angle by polar angles (θ_j, ϕ_j) of the field direction with respect to the C, K, D, and Q

coordinates. Then, nuclear spin matrices are transformed as:

$$I_x^Z = I_x^j \cos\theta_j \cos\phi_j + I_y^j \cos\theta_j \sin\phi_j - I_z^j \sin\theta_j, \quad (3)$$

$$I_y^Z = -I_x^j \sin\phi_j + I_y^j \cos\phi_j, \quad (4)$$

$$I_z^Z = I_x^j \sin\theta_j \cos\phi_j + I_y^j \sin\theta_j \sin\phi_j + I_z^j \cos\theta_j, \quad (5)$$

where j designates the one of the coordinates (C, K, D, Q).

When we applied the magnetic field parallel to the $\langle 110 \rangle$ direction , $(\theta_C, \phi_C) = (90°, 45°)$, two inequivalent Nb sites should appear as shown in the inset of Fig. 1. And, at least eighteen ^{93}Nb-NMR lines are expected to be observed. In this field direction, the field angle is expressed as $(\theta_{K,Q,D}, \phi_{K,Q,D}) = (35°, 0°)$ for A and B sites in the inset of Fig. 1, and $(90°, 45°)$ for C and D sites in Fig. 1.

The black dashed, red solid, green dotted, and blue dashed-dotted lines is a result of the simulation using $(\theta_C, \phi_C) = (87°, 38°)$, $K_{\rm iso} = 0.3\%$, $K_1 = K_2 = -0.1\%$, and $K_3 = 0.2\%$, respectively. Here we used $\nu_{\rm Q,Nb} = 1.82$ MHz and of $\eta_{\rm Nb} = 0$ [9]. In this case, the classical dipole contribution is obtained to be ≈ 10 Oe for this direction and is negligibly small in this experimental accuracy. For this field direction, four Nb sites A, B, C, and D give distinct lines. Thus, thirty-six ^{93}Nb-NMR lines are expected to be observed. The agreement between experimental and calculated lines is sufficiently good. Thus, we determined the field direction by analyzing the obtained ^{93}Nb-NMR line. The misalignment from the $\langle 110 \rangle$ direction is due to the setup of the sample rotator.

Then, we tried to assign ^{27}Al lines. As shown above, Al(3) site has a monoclinic local symmetry and there is one mirror plane that is parallel to one of $\langle 110 \rangle$ directions. In such a case, one of the EFG principal axes is perpendicular to the mirror plane and the rest axes are in the mirror plane. However, we found that ^{27}Al-NMR lines cannot be reproduced by using the obtained field angle of $\theta_C = 87°$, $\phi_C = 38°$ and using the previous NQR parameters $\nu_{\rm Q,Al(3)} = 1.53$ MHz and $\eta_{\rm Al(3)} = 0.17$ for Al(3) site measured at ≈ 2.8 T and 30 K [9]. To reproduce the ^{27}Al-NMR line profile, the NQR parameters should depend drastically on temperature in the temperature range of 30 K and 50 K. However, ^{27}Al- and ^{93}Nb-NQR studies revealed that the NQR parameters hardly depend on temperature below 50 K [8, 9]. Thus, we should reconsider the simulation of the powder NMR lines by taking account of contributions from the hyperfine and nuclear dipolar interactions.

Figure 2 displays the frequency-swept ^{27}Al-NMR lines obtained at 2.8 T and 60 K. A red solid line is a result of the simulation for Al(2) sites by using the NQR parameters $\nu_{\rm Q,Al(2)} = 2.28$ MHz and $\eta = 0.17$ previously obtained in Ref. [9]. The experimental line is well reproduced by the simulation, confirming the validity of the estimated NQR parameters. On the other hand, as shown by a green dashed line in Fig. 2, there is a slight discrepancy between the experiment and simulation for Al(3) site. As mentioned previously, we neglected the contributions of the anisotropic Knight shift and classical magnetic dipole field in the previous analysis [9], where these contributions are affected by the Curie-Weiss like temperature dependence of magnetic susceptibility. The dipole contribution is small for Nb and Al(2) sites as mentioned before. On the other hand, the contribution is significant at Al(3) site as shown above. In addition, the effect of the anisotropic shift should be taken into consideration. In this context, it is reasonable to consider that the contributions from the hyperfine and dipolar interactions affect temperature and field dependences of NMR spectrum. In fact, we can fit the line profile better by using $\nu_{\rm Q,Al(3),new} \approx 1.0$ MHz and $\eta_{\rm Al(3),new} \approx 0.4$. A blue dotted line is the result of the simulation by using $\nu_{\rm Q,Al(3),new}$ and $\eta_{\rm Al(3),new}$. Thus, obtained $\nu_{\rm Q,Al(3),new}$ and $\eta_{\rm Al(3),new}$ are considered to be reliable.

Finally, we reconsider the previous NQR results. In the previous analysis [9], as shown by black solid lines in Fig. 3, we reported the NQR lines at around 1.5 MHz and 3.0 MHz were reproduced by using $\nu_{\rm Q,Al(3)}$ and $\eta_{\rm Q,Al(3)}$. However, powder samples used in the previous NQR study [9, 11] contain a small but NQR detectable amount of $NbAl_3$ impurity. NQR parameters of Nb site in $NbAl_3$ is previously reported to be $\nu_{\rm Q,NbAl_3} \approx 2.9$ MHz [12]. Thus, we find the NQR signal at around 3.0 MHz does not originate from $PrNb_2Al_{20}$, but from $NbAl_3$ impurity. Instead, we reproduced an NQR signal at around 1.9 MHz by using $\nu_{\rm Q,Al(3),new}$ and $\eta_{\rm Al(3),new}$ as shown by blue solid lines in Fig. 3. The origin of the NQR

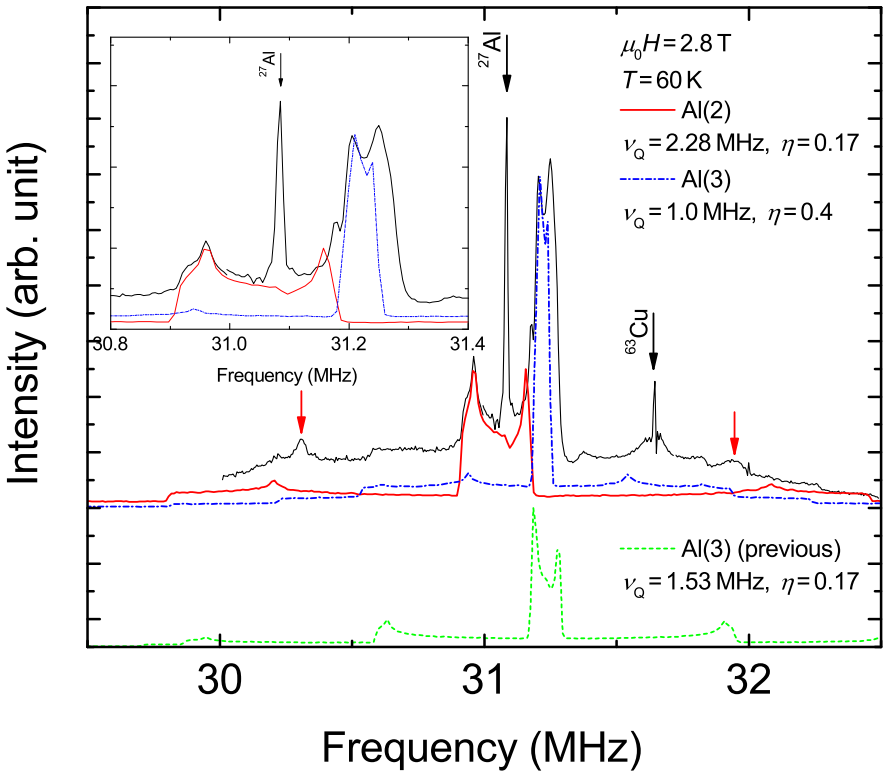

Figure 2. The ^{27}Al-NMR line obtained for a field of 2.8 T and 60 K. Red solid, green dashed, and blue dashed-dotted lines are the results of the simulation described in the text. Al and Cu signals designated by black arrows arise from the impurity and NMR coil. Peaks designated by red arrows are originate from ^{93}Nb in $PrNb_2Al_{20}$. The inset represents an enlarged view of the center of the NMR line.

line at around 1.5 MHz may be an experimental artifact. Further experimental confirmation of NQR lines are needed.

By using $\nu_{Q,Al(3),new}$ and $\eta_{Al(3),new}$, the assignment of ^{27}Al-NMR lines for a single crystal and the determination of the EFG axes are in progress. In addition, NQR signal search at below 2 MHz is also in progress.

4. Summary

We observed ^{93}Nb- and ^{27}Al-NMR signals of a single crystal $PrNb_2Al_{20}$. By using the previously reported NQR parameters, we reproduced the field angle dependence of the ^{93}Nb-NMR lines, while we could not reproduce the Al(3) lines by the previously obtained ^{27}Al(3)-NQR parameters. Thus, we reexamined the powder NMR and NQR spectra and obtained correct NQR parameters for Al(3) site to be $\nu_{Q,Al(3),new} \approx 1$ MHz and $\eta_{Al(3),new} \approx 0.4$. These results indicate the importance of the anisotropic hyperfine interaction and classical dipole field to analyze the temperature and field dependence of NMR lines in $PrNb_2Al_{20}$.

Acknowledgments

We gratefully thank Prof. H. Harima, Dr. S. Kitagawa, and Mr. T. Taniguchi for valuable discussions and helpful advice. This work has been supported by a Grant-in-Aid for Scientific Research on Innovative

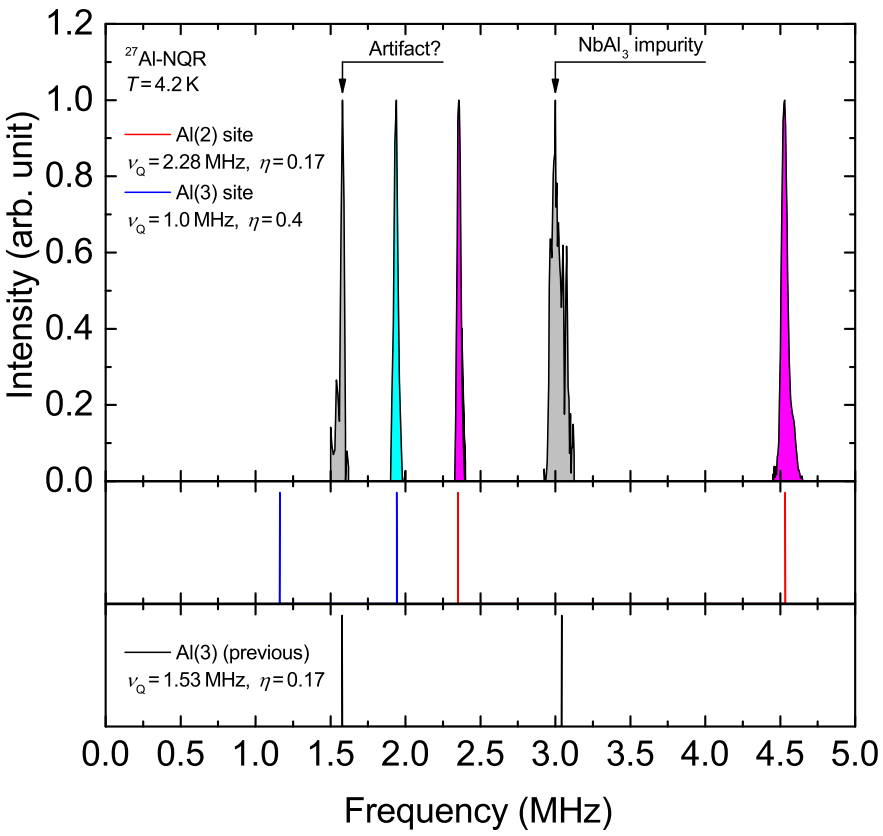

Figure 3. NQR lines obtained by using powder samples at 4.2 K. Intensity is normalized at each peak positions. Black solid lines are the result of the simulations for previously obtained NQR parameters for Al(3) site. This result is inconsistent with NMR results as discussed in the text.

Areas "J-Physics" (No. 15H05885) and Grants-in-Aid for Scientific Research (Nos. 26400359 and 15H05745) of the Ministry of Education, Culture, Sports, Science and Technology, Japan.

References

[1] Onimaru T, Matsumoto K T, Inoue Y F, Umeo K, Saiga Y, Matsushita Y, Tamura R, Nishimoto K, Ishii I, Suzuki T and Takabatake T 2010 *J. Phys. Soc. Jpn.* **79** 033704
[2] Onimaru T, Matsumoto K T, Inoue Y F, Umeo K, Sakakibara T, Karaki Y, Kubota M and Takabatake T 2011 *Phys. Rev. Lett.* **106** 177001
[3] Higashinaka R, Nakama A, Ando M, Watanabe M, Aoki Y and Sato H 2011 *J. Phys. Soc. Jpn.* **80** SA048
[4] Sakai A and Nakatsuji S 2011 *J. Phys. Soc. Jpn.* **80** 063701
[5] Sakai A, Kuga K and Nakatsuji S 2012 *J. Phys. Soc. Jpn.* **81** 083702
[6] Tsujimoto M, Matsumoto Y, Tomita T, Sakai A and Nakatsuji S 2014 *Phys. Rev. Lett.* **113** 267001
[7] Higashinaka R, unpublished.
[8] Kubo T, Kotegawa H, Tou H, Higashinaka R, Nakama A, Aoki Y and Sato H 2015 *J. Phys. Soc. Jpn.* **84** 074701
[9] Kubo T, Kotegawa H, Tou H, Higashinaka R, Nakama A, Aoki Y and Sato H 2015 *J. Phys.: Conf. Ser.* **592** 012093
[10] Tou H, Tsugawa N, Sera M, Harima H, Haga Y and Ōnuki Y 2007 *J. Phys. Soc. Jpn.* **76** 024705; 2007 *J. Phys. Soc. Jpn.* **76** 058001
[11] Kubo T, Kotegawa H, Tou H, Higashinaka R, Nakama A, Aoki Y and Sato H 2014 *JPS Conf. Proc.* **3** 012031
[12] Lue C S, Su T H, Xie B X and Cheng C 2006 *Phys. Rev. B* **74** 094101